DOI: 10.1002/asia.200800333

"Half-Bonds" in an Unusual Coordinated S_4^{2-} Rectangle

Anne Poduska,[a] Roald Hoffmann,*[a] Andrea Ienco,[b] and Carlo Mealli[b]

Dedicated to Professor Ryoji Noyori on the occasion of his 70th birthday

Abstract: The bonding of a rare S_4^{2-} rectangle coordinated to four transition metals (synthesized by Isobe, Nishioka, and co-workers), $[\{M_2(\eta^5\text{-}C_5Me_5)_2(\mu\text{-}CH_2)_2\}_2(\mu\text{-}S_4)]^{2+}$ (M=Rh, Ir) is analyzed. DFT calculations indicate that, while experiment gives the rectangle coordinated with its long edge parallel to Rh–Rh bonds and perpendicular to the Ir–Ir bonds, either orientation is feasible for both metals. Although rotation of the S_4 rectangle is likely a multi-step process, a calculated barrier of 46 kcal mol^{-1} for a simple interconversion pathway goes through a trapezoidal, not a square, transition state. An argument is presented, based on molecular orbital (MO) calculations, that the long S–S contacts (2.70 and 2.90 Å) in the rectangle are in fact two-center, three-electron bonds (or "half-bonds"). Moreover, the 2– charge on the S_4 rectangle is related to a Jahn–Teller distortion from a square to a rectangle. Finally, DFT is used to explore possible stable intermediates in the oxidative process giving these $M_4S_4^{2+}$ compounds: for Ir, the coupling of two $Ir_2S_2^{+}$ molecules appears feasible, as opposed to a possible two-electron oxidation of a neutral Rh_4S_4 molecule.

Keywords: half-bonds · Jahn–Teller distortion · quantum chemistry · sulfur bonding · transition metal

Introduction

In a number of ways, sulfur is a very accommodating element. It displays a wide range of oxidation states, from 2– in sulfides to 6+ in sulfates and, out of all the elements, sulfur has the largest number of allotropes.[1] Observed sulfur–sulfur bond distances also cover a wide range: they begin on the short side with S_2^{2+} giving a (calculated) triple bond of around 1.78 Å,[2] with a slightly longer distance of about 1.82 Å in S_2^{+} from both theory and experiment.[3–5] S–S distances increase to a typical single bond, around 2.05 Å (H_2S_2),[6,7] and head up to surprisingly long bonding contacts in the molecule S_6^{-} (2.63 Å)[8] and in the complex formulated as $[Cp^*Fe(\mu\text{-}S_2)_2FeCp^*]^{2+}$ (2.89 Å).[9] This range of bond distances does not mean sulfur bonds are weak: sulfur has the third-strongest homonuclear single bond, and its strength of 265 kJ mol^{-1} is third only to C–C (~330 kJ mol^{-1}) and H_2 (435 kJ mol^{-1}).[1,10]

Sulfur's versatility in bonding has presented both theoreticians and experimentalists with challenges in gaining understanding, even for the simplest problem of elemental sulfur allotropes. Classically, in all of these compounds, S should form two bonds to other S atoms; of course, there are many ways to do this. Some ground state structures—such as orthorhombic α-S_8 containing crown-shaped rings of S—are well-known, but the structure of other allotropes, such as S_4, for which perfectly good Lewis structures may be drawn, are enigmatic owing to a number of competitive geometries. Our paper, in fact, is concerned with S_4, not as an isolated molecule, but as a bridge in transition-metal complexes.

It is still disputed whether free S_4 exists as a ring (specifically, a rectangle or trapezoid) or as a linear structure.[11–13] The latest published studies conclude that the singlet trapezoid is the ground state, determined to be below the rectangle by a mere 1.6 kcal mol^{-1}.[14,15] It is likely that this molecule is quite flexible. Coordinated S_4 is found in a number of inorganic and organometallic compounds. Of course, coordination (especially to metals) can effectively transfer electrons, so that one may be dealing more with S_4^{2-} (or even $2S_2^{2-}$) than with S_4. An open-chain structure, the simplest structural proposal (we will see others in the course of this paper), is expected for S_4^{2-}, and indeed that is the way the

[a] Dr. A. Poduska, Prof. R. Hoffmann
Department of Chemistry and Chemical Biology
Cornell University
Ithaca, New York 14850 (USA)
Fax: (+1) 607-255-5707
E-mail: rh34@cornell.edu

[b] Dr. A. Ienco, Dr. C. Mealli
Istituto di Chimica dei Composti Organometallici, ICCOM-CNR
Via Madonna del Piano 10, 50019 Sesto Fiorentino, Firenze (Italy)

Supporting information for this article is available on the WWW under http://dx.doi.org/10.1002/asia.200800333.

fragment is found in, inter alia, $[MoS_8O]^{2-}$,[16] or in the solid state structure of Na_2S_4.[17]

An S_4 ring (neutral or dianionic) is much rarer. We do see a neutral rectangular S_4 ring appear as a partial structure in one geometry of a hypothetical isomer of S_8.[18] And it seems like some of these rare S_4^{2-} rings do exist, but are not easily recognized. For example, we recently reconsidered the structure of several transition-metal compounds with two disulfide units in them, $(\mu\text{-}S_2)_2$[19,20]: a triple-decker compound,[9] $[Cp^*Fe(\mu\text{-}S_2)_2FeCp^*]^{2+}$, and a chair-like $[L_2Cu(\mu\text{-}S_2)_2CuL_2](OTf)_2$ ($L_2 = Me_2NCH_2CH_2Ne_2$, OTf = trifluoromethanesulfonate).[21] We proposed that, even though the S–S contacts between the disulfide units are on the long side (2.74 and 2.89 Å, respectively), it makes great sense to think of these as containing a weak half-bond between the two disulfide units to form an unusual S_4^{2-} rectangle.

The impetus to our current study comes from another appearance of an S_4 rectangle in the organometallic literature.[22] Consider the two clusters, shown in Figure 1, here-

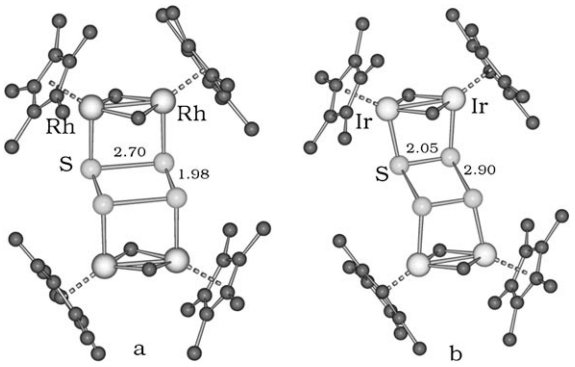

Figure 1. The experimental structures of a) $[\{Rh_2(\eta^5\text{-}C_5Me_5)_2(\mu\text{-}CH_2)_2\}_2(\mu\text{-}S_4)]^{2+}$, which we will refer to as "$Rh_4S_4^{2+}$" and b) $[\{Ir_2(\eta^5\text{-}C_5Me_5)_2(\mu\text{-}CH_2)_2\}_2(\mu\text{-}S_4)]^{2+}$, which we will call "$Ir_4S_4^{2+}$." The H atoms have been omitted for clarity.

after referred to as "$Rh_4S_4^{2+}$" and "$Ir_4S_4^{2+}$".[23,24] Aside from the relatively rare bridging methylene groups and parallel S–S and M–M bonds (S_2 units usually coordinate transition metals in the side-on configuration, as in $[Mo_2(S_2)_6]^{2-}$),[16] we see something even more unexpected. The S_4 unit (no implication, yet, of the formal charge it carries) is a rectangle, far from a square; and, remarkably, this rectangle is rotated by 90° in these two clusters that are clearly related both electronically and structurally. In $Rh_4S_4^{2+}$, we see the long S_4 edge oriented parallel to the Rh–Rh bonds, whereas in $Ir_4S_4^{2+}$, this edge is perpendicular to the Ir–Ir bonds. However, there is a similar deviation in both clusters from a square S_4: in $Rh_4S_4^{2+}$, the edges are 2.70 and 1.98 Å, whereas in $Ir_4S_4^{2+}$, the S–S distances are 2.90 and 2.05 Å—differences of 0.72 and 0.85 Å, respectively.

These two S_4-bridging compounds have several interesting aspects that we will explore in this paper. Why is the S_4 rectangle rotated—and can we say anything about the energy barrier or possible route to rotation? Why does this rare S_4 rectangle exist in the first place, and are there any electronic differences between the $Rh_4S_4^{2+}$ and $Ir_4S_4^{2+}$ complexes? Why does a rectangle—not a square—exist? Moreover, can theory help explain how these rings form experimentally? This discussion will be largely shaped by DFT and extended Hückel calculations: their details are described in the Computational Details section.

Calculations: Experimental Structure and Rotation of S_4 Rectangle by 90 Degrees

Let us first start our discussion with an exploration of the S_4 ring orientation. Our calculations find that both experimental structures of $Rh_4S_4^{2+}$ and $Ir_4S_4^{2+}$ are local minima, with slightly overestimated M–M bond distances (0.01 and 0.03 Å). The S–S contacts have larger errors (that probably reflect the very flat PES for residual S–S bonding over long distances): the short S–S bond is within 0.03 Å of the experimental structure, but the long S–S contact is overestimated by about 0.14 Å in the Rh compound and 0.20 Å in the Ir compound. Additional information about the accuracy of these bond distances is included in the Computational Details.

We also optimized the $Rh_4S_4^{2+}$ and $Ir_4S_4^{2+}$ clusters starting with the S_4 rectangle in the opposite orientation. We did this by exchanging Rh for Ir in the $Ir_4S_4^{2+}$ cluster (and the converse in the $Rh_4S_4^{2+}$ cluster). Interestingly, we found that the optimized structures maintained the S_4 orientation, and the M–M and S–S bond distances are within 0.06 Å of those with which the optimization began. Thus, the calculations for both complexes show two minima (Figure 2): the Rh_2 and Ir_2 metal fragments can bond effectively to either the long or the short side of the S_4 rectangle.

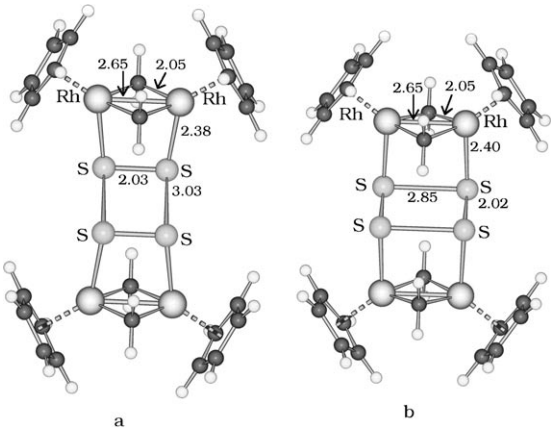

Figure 2. Drawings of the optimized $Rh_4S_4^{2+}$ complexes (a and b) highlighting the geometric parameters and the two different S_4 orientations.

What is the energetic difference between the two S_4 orientations? Our DFT calculations show that the most stable structure for both Rh and Ir is that with the long S–S bond parallel to the M–M axis (Figure 2b); however, the differences are less than 4 kcal mol^{-1} in each case. We do not wish

to attribute much significance to this preference; it may change with the level of the calculation.

If theory shows little thermodynamic preference for the S_4 orientation, why does experiment not give us both orientations for Rh and Ir? The experimental observation of two—not four—structures might arise from the influence of crystal packing: the $Rh_4S_4^{2+}$ counterions can be I^-, BF_4^-, or a combination of OH^- and Cl^-, whereas $Ir_4S_4^{2+}$ counterions are just Cl^-.[23,24] Another possible explanation (which we will address in detail) is that pairs of binuclear precursors can assemble in tetrameric units before oxidation, especially in the case of the rhodium species. And, as we will show later, whatever may be the kinetic preferences, a large activation energy prevents the rearrangement of one orientation of the $M_4S_4^{2+}$ product into the other orientation.

Kinetic factors might also be at work: however, a discussion about kinetics is particularly difficult, given the different (and likely complex) synthetic strategies for the Rh and Ir compounds. For example, two pathways have been shown to give $Rh_4S_4^{2+}$,[23,24] (Schemes 1a and b).

Reacting $[(RhCp^*)_2(\mu\text{-}SH)]X$ ($X = Cl$, BF_4, BPh_4) with oxygen in excess H_2S gives $[Rh_4S_4^{2+}][(OH^-)(Cl^-)]$; the counterions can be exchanged with BF_4^- upon precipitation with $NaBF_4$ (Scheme 1a). Alternately, reaction of the thiosulfito derivative $[(RhCp^*)_2(\mu\text{-}CH_2)_2(SSO_2\text{-}S{:}S')]$ with 1,2-diidoethane gives $[Rh_4S_4^{2-}][(I^-)_2]$ (Scheme 1b).

On the other hand, $Ir_4S_4^{2+}$ forms by reacting two "halves"—$[(IrCp^*)_2(\mu\text{-}CH_2)_2(\mu\text{-}S_2\text{-}S{:}S')]$[24–26] —at room temperature with alkyl chlorides (such as $CHCl_3$ and 1,1-Cl_2CHCH_3) (Scheme 1c).[24] The different pathways for the Rh and Ir complex could arise from the air-sensitivity of the Rh "half": although NMR and FAB mass spectrometry indicate it may have formed, isolation and single-crystal formation have not been possible.[27] We performed a geometry optimization and frequency calculation on this structurally unknown $Cp_2Rh_2(\mu\text{-}CH_2)_2(\mu\text{-}S_2)$ complex and we found that for the neutral molecule, the local minimum gives an S–S distance of 2.15 Å, similar to that of the Ir equivalent (Figure 3a). These binuclear species have been optimized also as monocations and as uncharged species in the triplet state (Figures 3b and 3c), which will be discussed later in this article.

Although different reactivity pathways (hence different kinetics) may lead to different S_4 orientations for the Rh and Ir species, an interesting question is whether a square S_4 transition state (TS) connects these two conformations—and, if so, where does it lie at in energy with respect to the rectangular geometry? A TS search for the interconversion of rectangular S_4 in the $Rh_4S_4^{2+}$ compound gives an asymmetric S_4 unit (Figure 4), with two adjacent sides having a shorter S–S distance (around 2.15 Å) and the other two sides having a longer S–S distance (2.81 and 2.92 Å).

Single-point DFT calculations on $Rh_4S_4^{2+}$ models with fixed distances in a S_4 square ring converge only in the triplet state for both short (2.02 Å) and long (3.02 Å) S–S sides. Their energies are 72 and 55 kcal mol^{-1} higher than the asymmetric S_4 TS, respectively (Figure 4). Energies of this

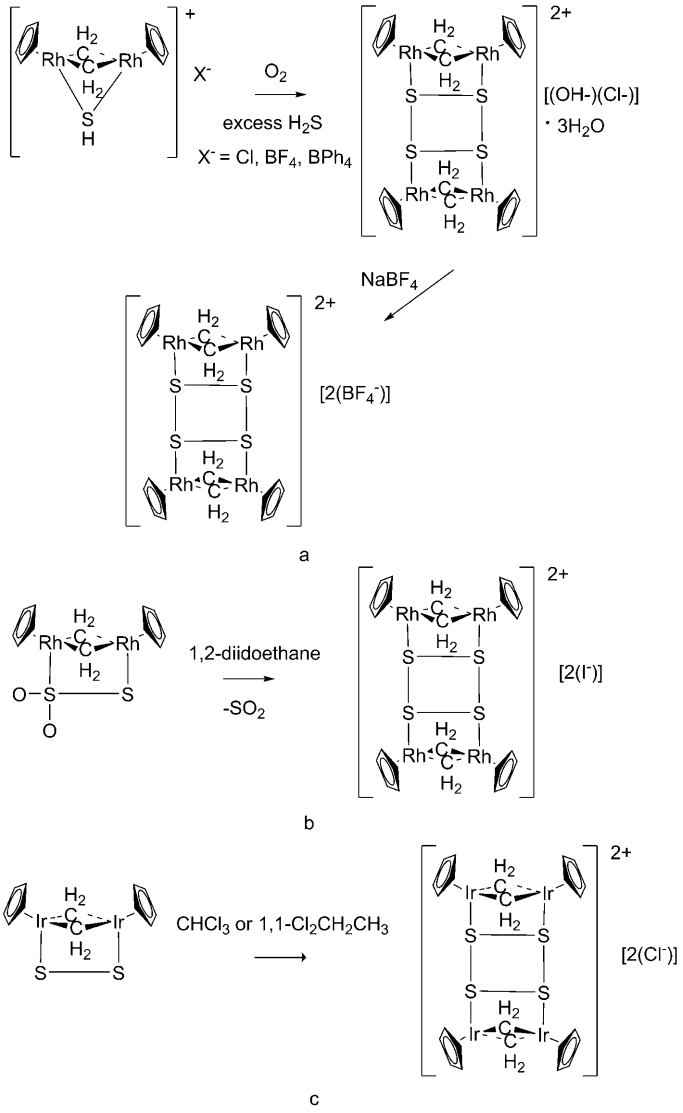

Scheme 1. Three different pathways for (a and b) $Rh_4S_4^{2+}$ and (c) $Ir_4S_4^{2+}$.

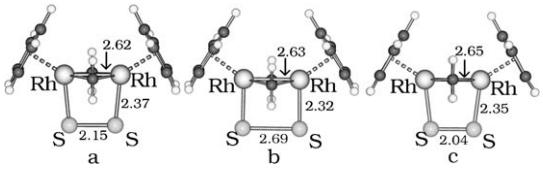

Figure 3. Optimized models of $Cp_2M_2(\mu\text{-}CH_2)_2(\mu\text{-}S_2\text{-}S{:}S')$: a) uncharged diamagnetic. b) uncharged with two unpaired electrons. c) monocations with one unpaired electron.

magnitude are significant: *this group of molecules really does not like a square S_4 ring.* In view of the seemingly simple rearrangement from a rectangle to a square (and the fact that we get triplet, not singlet, states for a calculated square geometry), these large energies are a sign of an orbital symmetry-forbidden reaction.

There is every sign of a Jahn–Teller distortion at work here. The detailed connection between the Jahn–Teller dis-

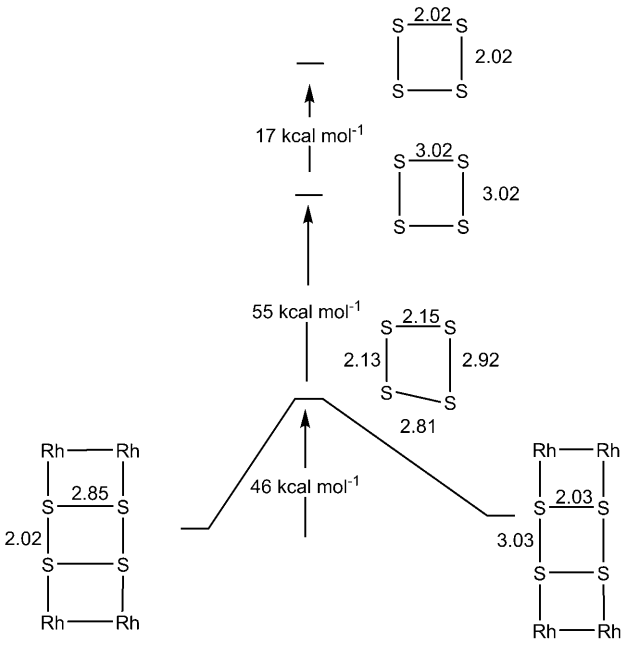

Figure 4. The energy of the (singlet) TS connecting the two orientations of the S_4 rectangle with Rh atoms (middle of diagram, lowermost structure), as well as the single-point energies of a coordinated square S_4 unit (in the triplet state) with long and short sides (middle of diagram, two uppermost structures). All energies are given relative to the $Rh_4S_4^{2+}$ structure on the left.

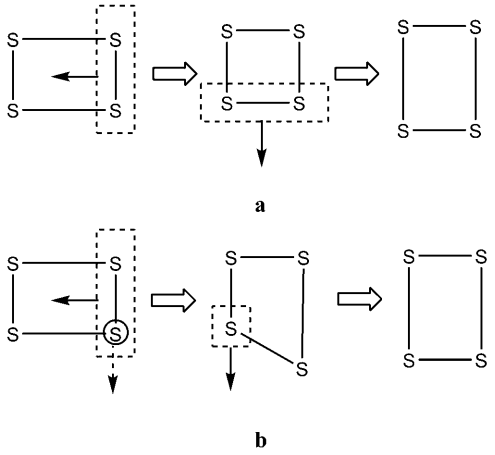

Figure 5. Two hypothetical scenarios that illustrate how a) a square and b) a trapezoidal transition state could connect the two orientations of the S_4 rectangle.

tortion and the high energy of the square S_4 geometry will be discussed below. Essentially, the S_4 ligand is really close to S_4^{2-} in this system, and just as the free S_4^{2-} is subject to a Jahn–Teller distortion, so does the coordinated ring gain much stability by distorting from a square to a rectangle.

Even the trapezoidal structure of Figure 4 is at high energy. This is likely to arise from the high deformation energy of the S4 σ-bonded framework of the rectangular geometry.

Although the potential energy surface of this system is complex, we can qualitatively understand how an asymmetric TS could connect the two orientations of the S_4 rectangle. If we had a square TS, we could imagine compressing the rectangle on one side to create a square (shown by the dashed box and arrow on the left-hand side of Figure 5a), and then elongating the square on the adjacent side to give the other orientation of the rectangle (right-hand side of Figure 5a).

Alternately, we can imagine the combined compression (shown by the arrow and dashed box on the left-hand side of Figure 5b) and elongation of one S–S side (shown by the movement of the circled S atom that follows the dashed arrow). This would give us the optimized trapezoidal TS (middle of Figure 4). To reach the other orientation of the rectangle, we would just need to elongate the other parallel S–S *bond* (shown by the dashed box and arrow, middle of Figure 5b) instead of elongating one *side* as we did in Figure 5a. Please note that this is just a qualitative sketch to help illustrate how a trapezoidal structure (provided that it is energetically accessible) could connect the orientation of these two rectangles.

In the SI, we also explore a variety of other arrangements of Rh and Ir atoms around the rectangle to see how stable this structure is relative to the metal environment. With one interesting exception, the S_4 rectangle turns out to be an invariant feature of these compounds. In short, it appears that the S_4 rectangular geometry is maintained, whether it bridges Ir or Rh atoms (or a combination thereof), or whether its long edge is oriented perpendicular or parallel to the M–M axes.

Our conclusions for this exploration of the S_4 orientation are as follows: the existence of opposite S_4 orientations in the $Ir_4S_4^{2+}$ and $Rh_4S_4^{2+}$ complexes is not easily explained, owing to their different synthetic pathways and high energy barrier for interconversion. Moreover, the simplest interconversion pathway with a square intermediate transition state appears unlikely. Additional synthetic approaches, possibly leading to alternative minima or isolation of intermediate structures that we will discuss later, are to be encouraged.

Electron Counting and Coordination for Rh and Ir

Our calculations seem to indicate that there is not much of an energetic preference for the orientation of the S_4 rectangle in the $Rh_4S_4^{2+}$ and $Ir_4S_4^{2+}$ compounds. Yet there is no doubt that a rectangle is preferred—but why? And what is the nature of the M–M and S–S bonding in these unusual molecules?

Let us begin with some simple electron counting for $Rh_4S_4^{2+}$ and $Ir_4S_4^{2+}$. We will take the S_4 ring as S_4^{2-} (a choice we will discuss later), with each S donating two electrons to each metal, and the Cp^-, as usual, as a six-electron anionic base. An electron-counting ambiguity exists when it comes to methylene ligands, depending on whether they are considered neutral or dianionic, a two or four-electron

donor. We will choose neutral CH_2 bridges, emphasizing their partial similarity to carbonyls in that they are two-electron σ donors and π acceptors.[28] Given the 2+ charge on M_4S_4, we then reach a formal +2 oxidation state and 17-electron count for each Group 9 metal. This is the right count for single M–M bonds, which is corroborated by the experimental bond distances of 2.66 Å in both complexes. Although this distance is slightly longer than the sum of the neutral Rh and Ir radii (2.50 and 2.54 Å, respectively)[29], it is shorter than the mean M–M bond distance (for both metals) of 2.75 Å, as given by a CSD search. Thus, a formal single M–M bond seems reasonable, especially considering the CSD shows that most Rh–Rh and Ir–Ir interactions fall within a 2.65–2.80 Å range.

In M_2X_2 complexes,[30,31] the bridge-supported, formally single M–M bond is affected by the donor/acceptor properties of the ligands, metal oxidation states, and M–X–M angle.[32–35] In the presence of methylene π-acceptor bridges, the electronic origin of the metal–metal bond can be rationalized by a strategy similar to that adopted for the highly debated Fe–Fe bond in the triply CO-bridged molecule $Fe_2(CO)_9$.[28,36] Namely, the formation of all the bridge bonds is first reconstructed in detail, and evidence for the M–M bond is consequently derived from the role of the MOs not directly involved in bridge bonding.

In the following section, we briefly outline the general electronic features of $M_2(CH_2)$ frameworks that are applicable for both the dinuclear and tetranuclear M_2S_2 and $M_4S_4^{2+}$ derivatives.

An Approach to Understanding $M_4S_4^{2+}$

In spite of the small energy difference between the two isomers, it is important to understand the different electronic structures for both S_4^{2-} orientations. One strategy is to employ a fragment molecular orbital (FMO) approach. We will first look at the orbitals of a $(CpMCH_2)_2^{2+}$ fragment which, relative to the M–CH_2 and M–M bonding, maintains constant features in all the derivatives. The fragment will be then interacted with either a strongly coupled S_2^{2-} unit (as in the stable and well-characterized complex $[(IrCp^*)_2(\mu\text{-}CH_2)_2(\mu\text{-}S_2\text{-}S\text{:}S')]$[24–26] of Figure 3a) or a weakened S_2^{2-} unit (as in the hypothetical complex $Rh_4S_4^{2-}$ or in the high-spin binuclear species of Figure 3b). The electronic structure of the potential binuclear precursors is fundamental for understanding their oxidation products, $M_4S_4^{2+}$ shown in Figure 1.

To start our FMO approach and to understand the M–M and $M_2(\mu\text{-}CH_2)_2$ bonding, we will interact the two methylene fragments with $(CpM\cdots MCp)^{2+}$. The 2+ charge is most appropriate to reach the neutral $Cp_2M_2(\mu\text{-}CH_2)_2(\mu\text{-}S_2)$ dinuclear molecule and, for convenience, we will limit the investigation to the rhodium species throughout the paper. Each $CpRh^+$ fragment is formally Rh^{II} d^7, and by the isolobal analogy, is equivalent to a non-planar $M(CO)_3$ or ML_3 fragment. Thus, we reach a local (distorted) octahedral geometry upon bonding $CpRh^+$ to the two bridging methylenes and one of the sulfurs in the S_2^{2-} unit.

On the left-hand side of Figure 6, we show the ten d-orbital combinations of both $RhCp^+$ fragments, as well as one s and p_x level (the remaining six s and p levels are not shown).

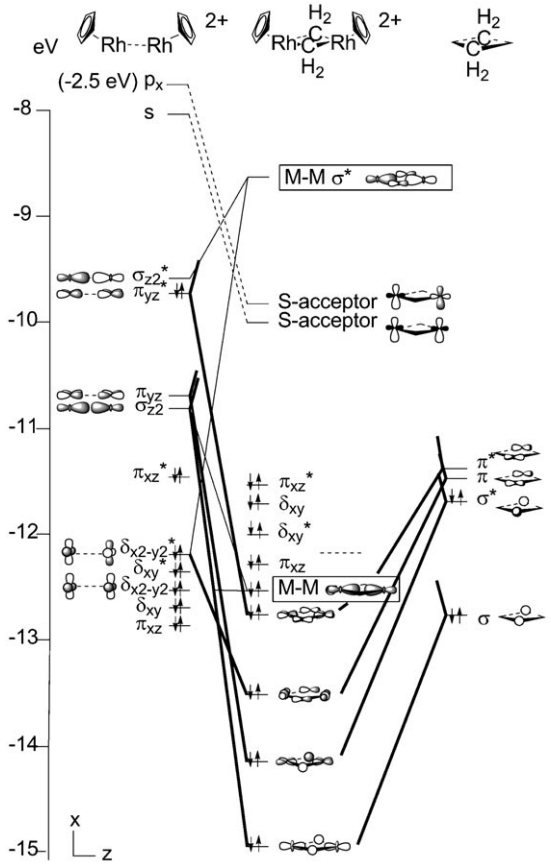

Figure 6. The interaction diagram for $CpRh{-}RhCp^{2+}$ and two CH_2 moieties.

The interactions of the metals with the methylene bridges induces significant mixing. The four combinations formed by z^2 and yz d orbitals lie somewhat higher than the other six d orbitals. This is because the presence of the Cp ligands forces their mixing with the higher-lying s and p orbitals.

Since the CH_2 groups have two lower σ-donor and two higher π-acceptor functions, the M–C bridge bonds result from two donations and two back-donations. The σ orbitals donate electron pairs into high and in-phase combinations of the metal σ_{z^2} and π_{yz} hybrids, both considered to be vacant. At the same time, the metal orbitals $\delta_{x^2-y^2}$* (lower) and π_{yz}* (higher) back-donate electrons into the CH_2 π and π* levels, respectively. For convenience, the higher π_{yz}* FMO is assigned two electrons and the lower σ_{z^2} one is left vacant.

After the interactions with the methylene bridges and eventually with the S_2^{2-} unit (the LUMO and LUMO+1 are ideally suited for this), the M–M bond is better understood. Since amongst the filled d orbitals $\delta_{x^2-y^2}$* strongly

contributes to M–C bridge bonding, and since both the FMOs σ_{z^2} and σ_{z^2}* are empty or participate in M–C bonding, there is a significant $x^2-y^2+z^2$ rehybridization. Essentially, the low-lying $\delta_{x^2-y^2}$ level becomes the primary M–M bonding orbital, while its antibonding partner is primarily σ_{z^2}*. Although identification of the M–M antibonding orbital is slightly complicated by the interconnected nature of M–M and M–C bonding, a Rh–Rh reduced overlap population (ROP) analysis seems to confirm that the LUMO+2 has the strongest M–M antibonding contribution (−0.218).

Forming $M_2S_2^{2+}$ With Long and Short S–S Bonds

Next, we illustrate in detail the interaction of the $(CpMCH_2)_2^{2+}$ fragment with an S_2^{2-} unit to give a neutral M_2S_2 fragment. This is important because we are interested in S_2^{2-} with both a long distance of 2.70 Å (as in $Rh_4S_4^{2+}$) and a short distance of 2.05 Å (as in $Ir_4S_4^{2+}$). The orbitals for these two S–S distances are given in Figure 7a and b.

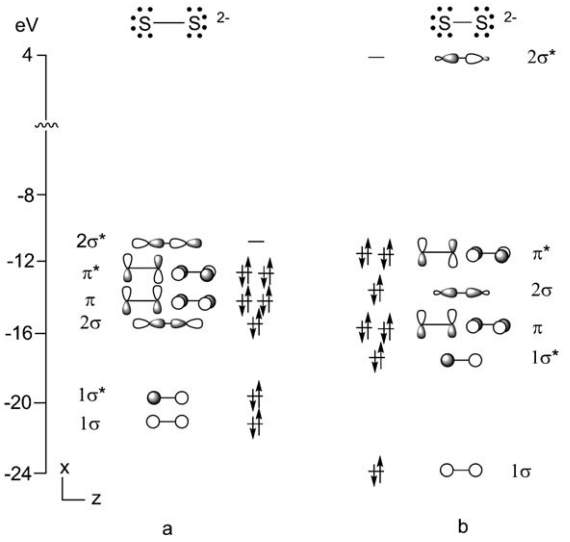

Figure 7. The levels of a S_2^{2-} molecule with two different distances of a) 2.70 Å and b) 2.05 Å.

In Figure 7a, the weak interaction between the S atoms does not induce the large level splitting observed in Figure 7b, where the short S–S distance causes significant dispersion. Particularly affected is the S–S 2σ* level, which lies about 15 eV higher in energy than in Figure 7a. Such a large difference is also a consequence of the greater sp hybridization at the shorter S–S distance: in fact, the 2σ* orbital is 34% s and 16% p, as compared to 2% s and 48% p at a long S–S distance.

The diagrams for the interaction of the $Cp_2Rh_2(\mu\text{-}CH_2)_2^{2+}$ species with the long and short S_2^{2-} unit are compared in Figure 8a and 8b.

We have omitted most of the Rh d combinations shown in Figure 6, as they undergo just minor shifts with the addition of the S_2^{2-}. In both cases, two Rh–S σ bonds are formed by

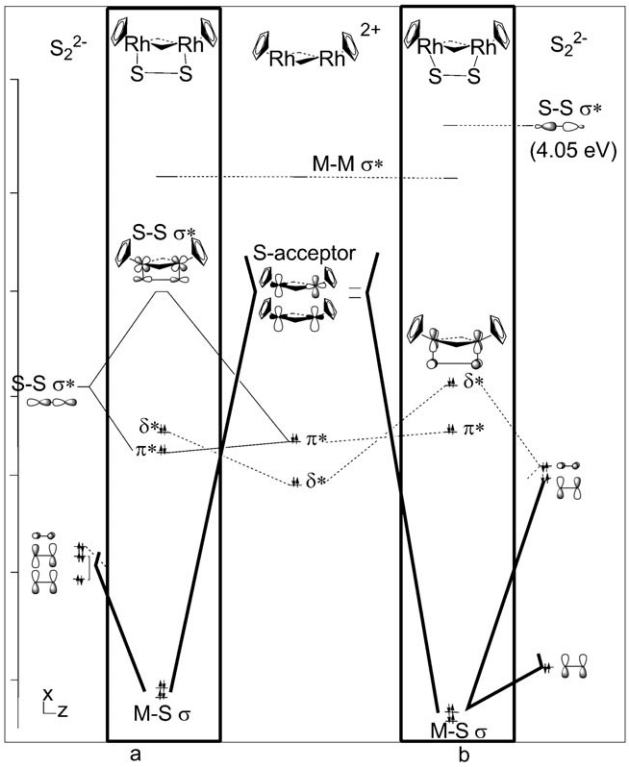

Figure 8. The interaction diagram between the important frontier orbitals of the Rh_2^{2+} and S_2^{2-} moieties to give Rh_2S_2 with an S–S distance of 2.70 Å (a) and 2.05 Å (b). Please note that, in both (a) and (b), there is a filled S_2^{2-} π* level that is not shown.

involving primarily the σ-acceptor hybrids of the M_2 fragment and the in-phase and out-of-phase combinations of S_2^{2-} p_x orbitals. Depending on the sulfur distance, there are slight (but not very significant) energetic differences in the filled Rh d orbitals upon coordination to either S_2^{2-}.

The most evident difference between the two cases is in the LUMO. When the S–S bond is short (Figure 8b), the LUMO is the M–M σ* level; when the S–S separation is large (Figure 8a), the LUMO is an antibonding mixture between a Rh–Rh π* combination and the S–S σ* orbital. This orbital has primarily sulfur, not metal, character. Thus, if this orbital were filled, we would have π back-donation from the metals into the S_2^{2-} unit (which we will see in the next section). This does not apply to the system with a short S–S distance (Figure 8b), for the S_2 σ* lies too high in energy.

Two points can be made for the "hypothetical" Rh_2S_2 isomer with the longer S–S distance. First, the Rh–S bonds have partial multiple bonding character as a result of the metal π back-donation into S–S σ* in the HOMO-1. Second, the HOMO–LUMO gap is not so large ($\Delta E \sim$ 1.3 eV), thus suggesting the possible access to a species with two unpaired electrons. We have calculated stable Rh_2S_2 and Ir_2S_2 triplet species (Figure 3b) with an elongated S–S distance (2.69 and 2.72 Å, respectively). This long S–S distance is consistent with filling an S–S σ* orbital. But these triplet

species are about 30 kcal mol^{-1} higher than the singlets (see Figure 3) and their accessibility, although consistent with S–S elongation, remains questionable.

(Schematically) Interacting the Two Halves of $Rh_4S_4^{2+}$ and $Ir_4S_4^{2+}$

Having clear orbital pictures of the binuclear M_2S_2 components, we are in a position to assemble fragments of the observed chair-like tetramers of $Rh_4S_4^{2+}$ and $Ir_4S_4^{2+}$. We begin with Figure 9, in which we interact (along the y axis) two "hypothetical" binuclear $Rh_2S_2^{+}$ species with an S–S distance of 2.70 Å. For each fragment we only show M–M σ* (as expected, the M–M bond is unaffected by tetramerization) and the S–S σ_z*, σ_y, and σ_y* orbital combinations.

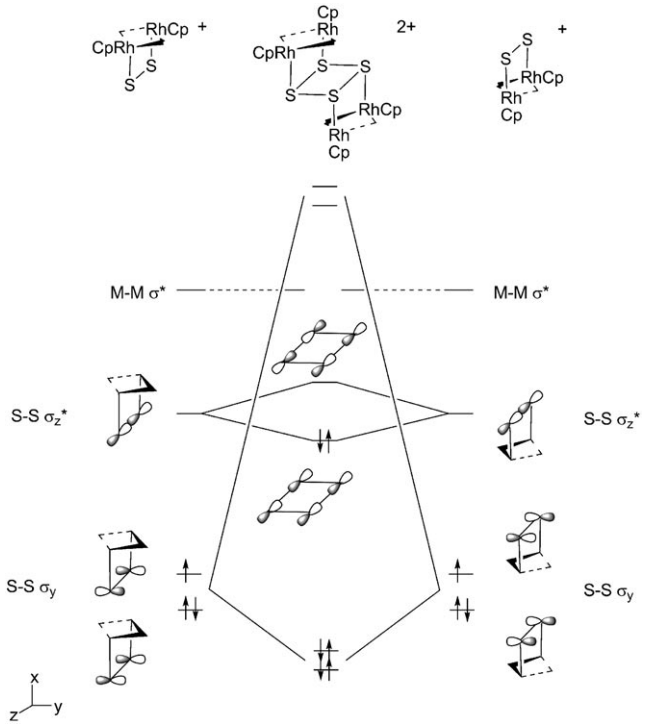

Figure 9. The essence of the $Rh_4S_4^{2+}$ interaction diagram with an S–S distance of 2.70 Å parallel to the M–M axis.

The two p_y combinations are most affected by the strong coupling, eventually leading to S–S separations as short as 1.98 Å. The S p_y antibonding combinations are high-lying and depopulated. The S–S σ_z* orbitals interact to form π and π* levels, which are the HOMO and the LUMO of the tetranuclear complex. The HOMO is π-bonding along the y-axis, which is in line with our S–S distance of 1.98 Å that is slightly shorter than a typical S–S bond of about 2.05 Å. Population of one of these σ* MOs reduces the S–S bond order in the z-direction to give two "half-bonds": that is, two two-center, three-electron S–S σ bonds.

To put it another way, we have a strong interaction of two sets of S-based radicals along the y direction, and a weaker interaction of S-based radicals along the z-direction. *The outcome is a 10 σ-electron system with four electrons (two full S–S bonds) along y, six electrons (two three-electron weaker σ bonds) along z.* The M–M bonding is unaffected, as the M–M σ* orbitals are empty.

Now let us look at what happens with when the long S–S distance is perpendicular to the Rh–Rh axis, as in the actual $Ir_4S_4^{2+}$ species. In this scenario, we now have an S–S distance of 2.05 Å parallel to the M–M. We again show a schematic diagram that carries the essential physics in Figure 10.

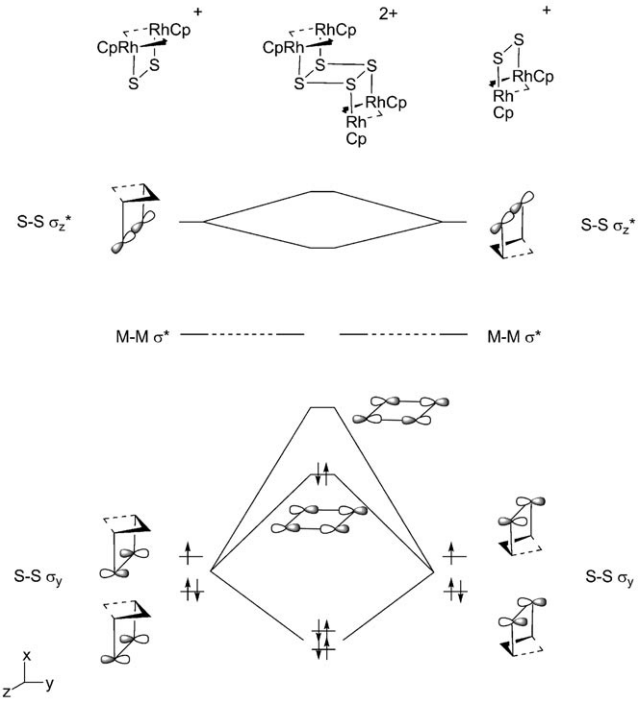

Figure 10. The essence of the $Rh_4S_4^{2+}$ interaction diagram with an S–S distance of 2.05 Å parallel to the M–M axis, as found in $Ir_4S_4^{2+}$.

To begin with, at the shorter S–S distance in $M_2S_2^{+}$, the S–S σ_z* lies very high in energy. The interaction of the two S_2 units along y is now even weaker than in Figure 9 because of the longer separation between the S_2 units (2.90 Å). Therefore, the antibonding combinations made up from S–S σ_y components do not rise as high as they did in Figure 9.

The net result is again a 10-electron S–S system, *but the S–S "half-bonds" are along y.* We note that the HOMO, although σ-antibonding in the y direction, is π-bonding in the z direction.

We see then, that for a short S–S bond parallel to the M–M axis, the σ_y splitting is small and we have filling of one σ_y* orbital to give two three-electron bonds along the y axis. Conversely, for long S–S bonds parallel to the M–M axis, we have a strong interaction between the sulfur σ_y orbitals, pushing the antibonding levels high in energy, causing one σ_z* level to be filled instead and giving "half-bonds" along the z-axis.

Understanding the Bonding in the S_4^{2-} Rectangle

These S–S "half-bonds" can be understood in several ways. First, three Lewis structures illustrate the possible scenarios in Figures 11a–c. One full S–S bond is broken (this is the typical situation of open tetrasulfido dianions) or two S–S bonds are "half-broken," going to three-electron S–S bonds (formal bond order 0.5).

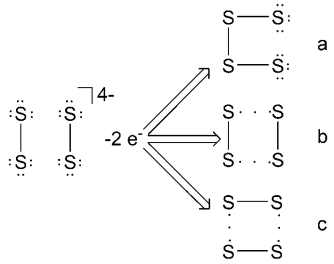

Figure 11. Three different electron distributions when removing two electrons form two disulfide units: a) breaking of one S–S bond, b) and c) forming two three-electron S–S σ bonds.

We can also understand the three-electron σ bonds (and the two orientations of the S_4^{2-} rectangle) from the viewpoint of a Jahn–Teller distortion from a square. To see this, let us first start with an isolated square S_4 and see what happens when we place a 2– charge on it. A single-point calculation on a neutral square S_4, having a modest S–S single bond distance of 2.05 Å, with B3LYP/6-311++G**, gives the resulting energy levels in Figure 12a. For clarity, we have not included here the orbital pictures for each MO. The filled levels are the equivalent from a localized viewpoint of four S–S σ bonds, four S–S π lone pairs, and four S–S in-plane π lone pairs.

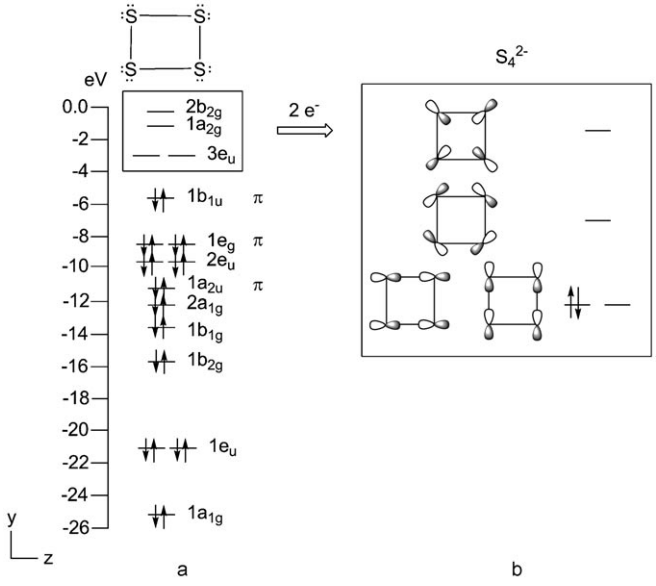

Figure 12. a) The energy levels for neutral S_4 at B3LYP/6-311++G**, with a S–S bond distance of 2.05 Å. We have identified the $1b_{1u}$, $1e_g$, and $2e_u$ orbitals as the out-of-plane π system. b) The S–S σ* for S_4^{2-}.

A 2– charge on S_4 creates the situation for a first-order Jahn–Teller (JT) distortion, for the degenerate $3e_u$ levels are half-filled. And what do these orbitals look like? In Figure 12b, we show the four highest MOs of S_4^{2-} in D_{4h} symmetry. We recognize these e_u orbitals as the HOMOs of $Rh_4S_4^{2+}$ and $Ir_4S_4^{2+}$. The relationship of these four orbitals to a localized picture can be gleaned from writing the four localized σ* levels (Figure 13a) and the four symmetry-adapted $b_{2g}+a_{2g}+e_u$ combinations derived from them (Figure 13b).

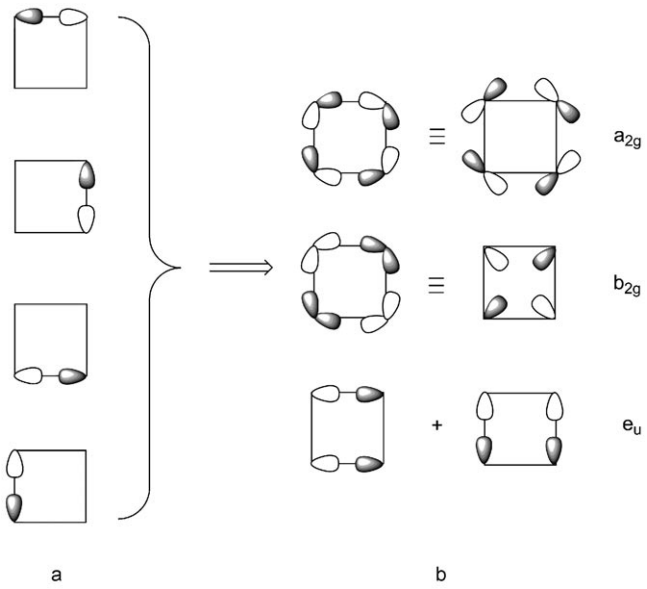

Figure 13. Localized S_4 σ* levels (a) and their delocalized equivalents (b).

The two e_u components are σ antibonding and π bonding along perpendicular directions. The workings of a Jahn–Teller distortion, following the double occupation of one or the other component of e_u, is now apparent in Figure 14.

If we elongate along the z axis, lowering the symmetry from D_{4h} to D_{2h}, we have a splitting of the $3e_u$ level shown in Figure 14c. The lower MO has maintained its π-bonding character and decreased the σ* interaction, whereas the opposite holds for the higher MO. If we elongate along the y axis, now we see a reversal as to which MO is lowered in energy, shown in Figure 14a, but otherwise a parallel behavior. The net result is a typical JT surface, of two intersecting potential energy curves in a state diagram.[37]

More Thoughts on the Two-Electron Oxidation Process

To understand the electronic structure of $M_4S_4^{2+}$, we theoretically assembled two M_2S_2 molecules by subtracting one electron from each dinuclear unit (formally at S_2^{2-}). Since the metal geometry is almost identical in the known structures of $Ir_2S_2^{0}$ and $Ir_4S_4^{2+}$, we believe that the oxidation

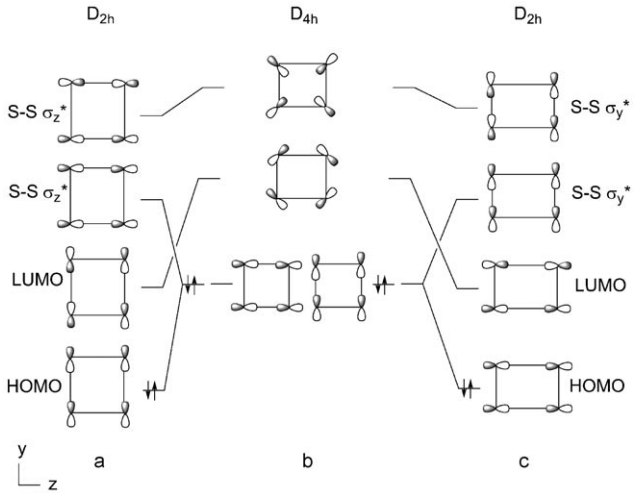

Figure 14. The potential first-order JT distortion in S_4^{2-}, with (a) being the orientation in $Ir_4S_4^{2+}$, (b) being the undistorted S_4^{2-} square, and (c) being the orientation in $Rh_4S_4^{2+}$.

mainly occurs at the S_2^{2-} units to form the S_4^{2-} ring. But there are open questions about the oxidative mechanism, since we do not know whether a one-electron oxidation of each Ir_2S_2 unit is the first event (followed by coupling of two radical complexes) or whether two electrons are simultaneously removed from two Ir_2S_2 molecules approaching each other.

Moreover, there are other, less simplistic approaches that involve other co-reagents. In the iridium case, the presence of alkyl chlorides at room temperature prompts the dimerization of the Ir_2S_2 units.[24] The rhodium case is more complicated because the pathway toward $Rh_4S_4^{2+}$ seems to involve binuclear species containing SH and SSO_2 groups (that have been experimentally characterized).[23,24] If the latter are actual intermediates, rather than side-products, a detailed experimental and/or theoretical mechanistic study would be necessary to describe the steps that eventually lead to the known $Rh_4S_4^{2+}$ isomer. As shown later (vide infra), we have computationally analyzed an alternative process that involves the formation of a fully reduced tetranuclear precursor $Rh_4S_4^{0}$, which, upon oxidation, could lead to the final $Rh_4S_4^{2+}$ product.

We believe that, by removing an electron apiece from two Ir_2S_2 molecules, radical coupling could be one viable synthetic pathway. This belief is based on our optimization of the monocation $[CpM(\mu\text{-}CH_2)_2(\mu\text{-}S_2)_2MCp]^+$, which is a minimum for both the Rh and Ir metals (Figure 3c). Moreover, the singly occupied molecular orbital (SOMO) maintains the features of the HOMO of the neutral M_2S_2 molecule in Figure 8b, that is, it is antibonding between metal δ* and S_2 π* orbitals.

We also see the feasibility of this one-electron oxidative pathway by calculating the evolution of the frontier orbitals as two Ir_2S_2 molecules approach each other to form $Ir_4S_4^{2+}$. In principle, the four-electron repulsion between the approaching sulfur atoms (if it is not compensated by other attractive interactions) should keep the S–S distances large. However, if the oxidant removes an electron from each HOMO of Ir_2S_2, the coupling mechanism could be triggered because it is favorable for the $Ir_2S_2^{+}$ molecules to get closer to each other.

We see in the Walsh Diagram (Figure 15) how energetically favorable it is to remove electrons from the two Ir_2S_2 units before coupling. On the left-hand side of the diagram,

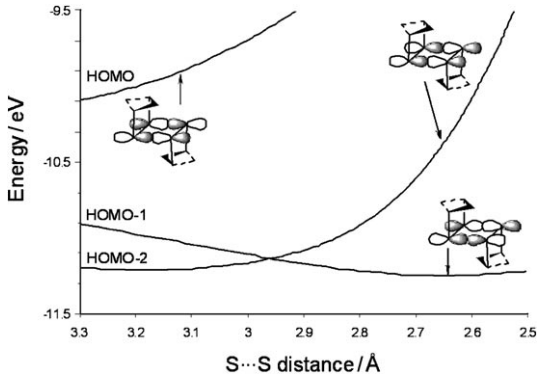

Figure 15. A Walsh diagram showing the evolution of the frontier MOs for two interacting $Ir_2S_2^{0}$ units. The out-of-phase combination of the HOMO-2 S_2^{2-} π levels progressively acquires destabilizing σ* character and, below 2.95 Å, becomes the HOMO of $Ir_4S_4^{2+}$.

we have the two neutral Ir_2S_2 molecules at a large distance (3.3 Å); on the right-hand side, we have the Ir_4S_4 molecule with an S–S distance of 2.5 Å between the two fragments. We can see that as the molecules approach each other, the HOMO of the $Ir_2S_2\cdots Ir_2S_2$ complex rises in energy very quickly. And, interestingly, the HOMO-1 lowers in energy because it has sulfur σ-bonding character between the fragments. Thus, a two-electron oxidation of the $Ir_2S_2\cdots Ir_2S_2$ system at a large separation would favor the approach of the two independent molecules.

We also see something interesting as the separation decreases: around 2.95 Å, we have a level crossing between the HOMO-1 and HOMO-2. A MO that is π bonding and σ* sharply rises in energy—and this MO is the HOMO of the $Ir_4S_4^{2+}$ molecule, shown in Figure 10.

Thus, on decreasing the S–S distance between the two Ir_2S_2 fragments even more, this Walsh Diagram suggests that another two-electron oxidation could give a stable $Ir_4S_4^{4+}$ molecule, which could potentially give an S_4 geometry closer to a square. Our DFT calculations show that $[\{Ir_2(\eta^5\text{-}C_5H_5)_2(\mu\text{-}CH_2)_2\}_2(\mu\text{-}S_4)]^{4+}$ is a minimum (Figure 16). However, the S_4 fragment is not square: this is likely owing to unequal metal–sulfur π- and δ-backdonation, for the S_4 unit remains rectangular, albeit with more equalized S–S sides of 2.16 and 2.54 Å.

So, for the $Ir_4S_4^{2+}$ species, it seems as though a one-electron oxidation of Ir_2S_2 units and subsequent coupling could be a viable route to its formation. For $Rh_4S_4^{2+}$, however, this route seems less likely since the Rh_2S_2 species is somewhat unstable (it might explain why its crystal structure was

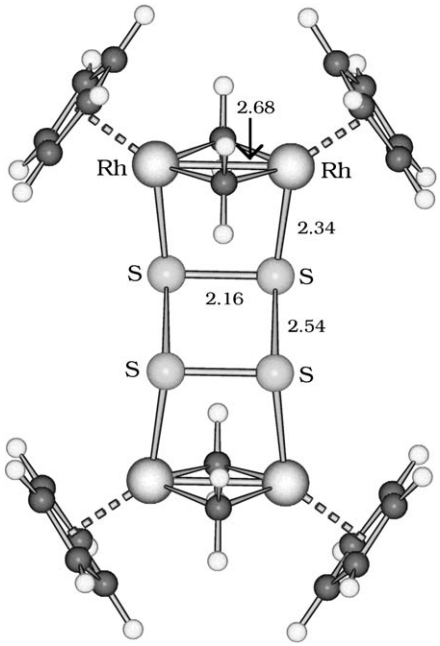

Figure 16. Optimized structure of $[\{Rh_2(\eta^5\text{-}C_5H_5)_2(\mu\text{-}CH_2)_2\}_2(\mu\text{-}S_4)]^{4+}$.

never determined) and there are likely oxygenated intermediates toward $Rh_4S_4^{2+}$. However, we find that a least-motion oxidative coupling of two S_2^{2-} ligands might still be possible. In fact, we minimized at the DFT level a stable and uncharged $Rh_4S_4^0$ species as a reasonable precursor (see Figure 17a). Regardless of the strong repulsion between the two disulfide ligands, the neutral molecule can accommodate two parallel S_2^{2-} units, separated by as much as 4.30 Å (i.e., well above the 3.68 Å sum of the sulfur van der Waals radii).

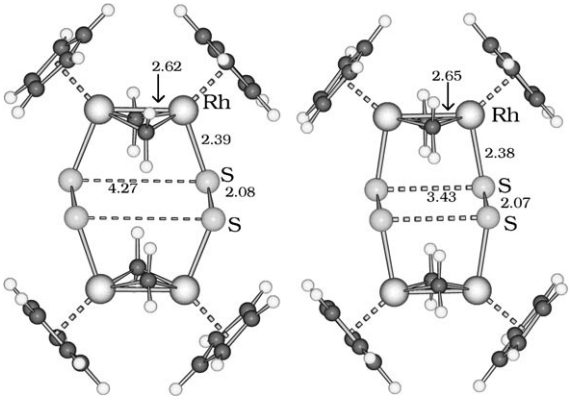

Figure 17. a) Optimized structure of $[\{Rh_2(\eta^5\text{-}C_5H_5)_2(\mu\text{-}CH_2)_2\}_2(\mu\text{-}S_4)]^0$ and b) $[\{Rh_2(\eta^5\text{-}C_5H_5)_2(\mu\text{-}CH_2)_2\}_2(\mu\text{-}S_4)]^+$.

From this structure, two stepwise oxidations could occur, for the doublet $Rh_4S_4^+$, presented in Figure 17b, is also a minimum. In the latter, the separation between the S_2 units is reduced to 3.43 Å, which is normally taken as a non-bonding value. However the S–S distance decreases by 0.87 Å, suggesting that the removal of one electron decreases the electron repulsion and perhaps attractive forces between the two S_2 units might be triggered. And, if a bond order of 0.5 applies in $Rh_4S_4^{2+}$, we then see two "quarter-bonds" for the S_4^{3-} ring in $Rh_4S_4^+$.

In $Rh_4S_4^0$, the connectivities of the $Rh_2(\mu\text{-}CH_2)_2$ framework are maintained with some minor structural rearrangements. The Rh–Rh distance barely shortens from 2.65 Å (Figure 2a) to 2.62 Å (but in $Rh_4S_4^+$ is again 2.65 Å); however, the methylene groups pucker opposite to the Cp ligands. In this manner, the metal σ hybrids (those accepting the S electrons) reorient but still allow the two parallel S_2^{2-} units to act as donors.

The $Rh_4S_4^0$ adduct is thermodynamically more stable than two discrete Rh_2S_2 units by about 13 kcal mol^{-1}, a result that seemed exciting because it would account for different synthetic routes to $Rh_4S_4^{2+}$ and $Ir_4S_4^{2+}$, respectively. However, calculations also show that a $Ir_4S_4^0$ minimum lies lower in energy (by -11 kcal mol^{-1}) relative to two isolated $Ir_2S_2^0$ units. Thus, at the moment, the difference between the synthetic routes for rhodium and iridium is not crystal clear. Nonetheless, our latest computational finding indicates the possibility of two straightforward, yet alternative, least motion oxidative pathways. Since the final products are different and not interconvertable species, a reasonable possibility is that the presumably metastable and electron rich $Rh_2S_2^0$ is kinetically less inert than the iridium to the coupling of two units before oxidation.

A Related Compound

A molecule without a chair-like geometry but having two bridging parallel main-group atoms (similar to that in Figure 17) exists, containing cyanide in place of S_2 linkers (Figure 18).

By reacting $Hg(CN)_2$ with a molecule similar to Isobe and Nishioka et al.'s dinuclear precursor—a $Cp^*_2Rh_2(\mu\text{-}CH_2)_2^{2+}$ core with one $-CH_3$ and one $-CH_2CN$ ligand instead of the $\eta^1\text{-}\eta^1\text{-}\mu_2\text{-}S_2^{2-}$ unit—a tetranuclear dication is formed.[38] Despite it sharing the same charge as $Rh_4S_4^{2+}$, there is not a four membered ring connecting the pairs of bonded metals in $[\{(C_5Me_5Rh\text{-}\mu\text{-}CH_2)_2\}_2(\mu\text{-}CN)_2]^{2+}$, nor does it have a chair-type structure. These differences occur because each cyanide ligand has collinear lone pairs, and the orthogonal p_π orbitals are involved in C–N triple bonding.

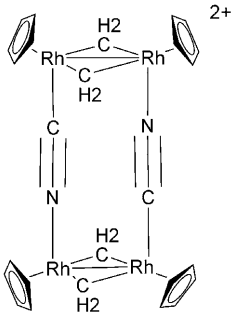

Figure 18. The dicationic complex $[\{(C_5Me_5Rh\text{-}\mu\text{-}CH_2)_2\}_2(\mu\text{-}CN)_2]^{2+}$.

With respect to our optimized species $M_4S_4^0$, $M_4S_4^{2+}$, and $M_4S_4^{4+}$ that we just mentioned, the cyanide-bridged molecule has eight, six, and four electrons less, respectively. We can understand a connection among all of these structures as illustrated in Figure 19,

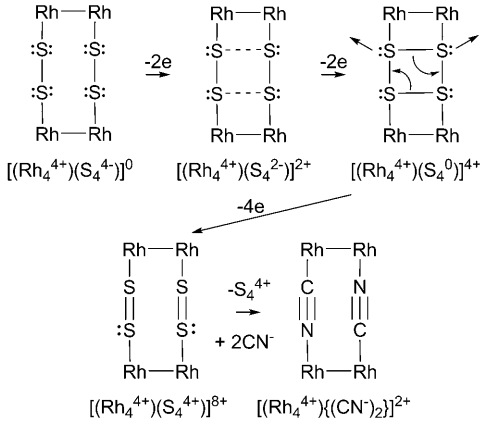

Figure 19. A series of two-electron oxidations and substitution of cyanide groups for S_2 bridges. These depictions do not take into account any changes in bond lengths as electrons are removed.

with a series of two- and four-electron oxidations of the Rh_4S_4 neutral species.

Initially, we begin with a neutral Rh_4S_4 unit, which does not have a S_4^{2-} ring, just two bridging disulfide groups (which we have written as S_4^{4-}), which serve as two-electron donors to each Rh. Removing two electrons to give $Rh_4S_4^{2+}$ forms the S–S "half-bonds" in S_4^{2-}; another two-electron oxidation gives four full S–S bonds in the resulting $Rh_4S_4^{4+}$ species.

Removing another four electrons to give the hypothetical $Rh_4S_4^{8+}$ molecule or the real $[Rh_4(\mu\text{-}CN_2)]^{2+}$ favors the formation of two additional bonds between the four central bridging atoms. Since this is achieved by breaking down the ring structure (namely by losing the single bonds parallel to the M–M vectors), the other two bonds must be transformed into triple bonds. This is hardly possible with parallel S_2^{2+} units, but their substitution with isovalent CN^- species is fully compatible with such a picture.

Conclusions

It appears that an S_4^{2-} rectangle in $Rh_4S_4^{2+}$ and $Ir_4S_4^{2+}$ can be bound in two ways, with the short S–S bond either parallel or perpendicular to the M–M axis. Our DFT calculations, together with a qualitative MO analysis, predict the existence of isomeric $Rh_4S_4^{2+}$ and $Ir_4S_4^{2+}$ complexes, only one of which (in each pair) has been made to date. We trace the presence of both orientations to a Jahn–Teller distortion from a square, and show that a 2– charge on S_4 favors this distortion. This S_4^{2-} rectangle has two S–S σ bonds and two three-electron S–S σ* bonds. This is true in both S_4 orientations found in $Rh_4S_4^{2+}$ and $Ir_4S_4^{2+}$, and in either case we find a formal M–M single bond.

We also analyzed the electronic features of each $M_4S_4^{2+}$ isomer to get valuable hints about their formation. For instance, we saw that the least-motion interconversion pathway through a square transition state is not likely. A trapezoidal geometry appears to be the lowest transition state but it is also disfavored by rather high energies. While for $Ir_4S_4^{2+}$ the formation of the S_4^{2-} unit from two disulfides seems to follow a least motion oxidative pathway, for $Rh_4S_4^{2+}$ one should, in principle, rely on the experimental indications of oxygenated intermediates.[24] Unfortunately, we could not provide any computational validation of such complex routes. On the other hand, DFT calculations suggest that two Rh_2S_2 units may be assembled in an experimentally undetected tetranuclear unit $Rh_4S_4^0$. From this, a least motion oxidative coupling of the S_2 units (stepwise) may occur with the ultimate formation of the observed $Rh_4S_4^{2+}$ species. Unfortunately, the rather similar computational outcome for analogous rhodium and iridium species does not allow establishing with precision the factors which ultimately differentiate the type of reactivity. Most likely, even small differences in electronegativity (orbital energies), as well as entropy factors and kinetic behavior are responsible for the presence of either isomer.

Computational Details

Structural optimisations were carried out with hybrid density functional theory (DFT) using the Gaussian03 suite of programs.[39] The method used was Becke's three-parameter hybrid exchange-correlation functional[40] containing the nonlocal gradient correction of Lee, Yang and Parr (B3LYP).[41] The nature of the optimized structures were confirmed by calculations of the frequencies. The Stuttgart/Dresden effective core potential was used for metals.[42] The basis set used for the remaining atomic species was the 6-31G(d, p).[43] The qualitative MO interpretation has been developed with the help of the EHMO-based CACAO package.[44] Coordinates of all the optimized species are given in the SI.

For DFT studies on organometallic Rh–S and Ir–S clusters,[45–47] substantial errors are typical in the S–S lengths, especially for particularly weak bonds. Whether B3LYP or B3PW91 is used, or if the transition metal basis set is LANL2DZ or a Stevens ECP plus double zeta polarization, or if the sulfur basis goes up to 6-31+G*, the typical discrepancy between theory and experiment is around 0.10 Å. Studies on sulfur allotropes fare slightly better, however. A UB3LYP/LANL2DZ calculation on S_2 overestimates the experimental distance of 1.88 Å by 0.09 Å (4% error), and six other basis sets used give an error range of 2.5–5%.[48] Other studies on higher-order sulfur allotropes give errors as small as 0.1% with MP4/6-31G* and up to 4% with triple-zeta and d-type polarizations.[11,13]

Acknowledgements

AP and RH are grateful to the National Science Foundation in support of this work through the grant NSF CHE-0613306. The group in Florence kindly acknowledges CINECA for the computing time provided under the agreement with CNR.

[1] N. N. Greenwood, A. Earnshaw, *Chemistry of the Elements*, *2nd ed.*, Butterworth-Heinemann, Boston, **1997**.
[2] G. H. F. Urban, M. Diercksen, M. Jurek, *Mol. Phys.* **1998**, *94*, 199.
[3] A. J. Capel, J. H. D. Eland, R. F. Barrow, *Chem. Phys. Lett.* **1981**, *82*, 496.
[4] J. M. Dyke, L. Golob, N. Jonathan, A. Morris, *J. Chem. Soc. Faraday Trans. 2* **1975**, *71*, 1026.
[5] D. J. Grant, D. A. Dixon, J. S. Francisco, *J. Chem. Phys.* **2007**, *126*, 144308.

[6] G. Winnewisser, M. Winnewisser, W. Gordy, *J. Chem. Phys.* **1968**, *49*, 3465.
[7] M. Winnewisser, J. Haase, *Z. Naturfosch.* **1968**, *23*, 56.
[8] B. Neumüller, F. Schmock, R. Kirmse, A. Voigt, A. Diefenbach, F. M. Bickelhaupt, K. Dehnicke, *Angew. Chem.* **2000**, *112*, 4753; *Angew. Chem. Int. Ed.* **2000**, *39*, 4580.
[9] H. Brunner, W. Meier, J. Wachter, E. Guggolz, T. Zahn, M. L. Ziegler, *Organometallics* **1982**, *1*, 1107.
[10] R. Steudel, *Angew. Chem.* **1975**, *87*, 683; *Angew. Chem. Int. Ed. Engl.* **1975**, *14*, 655.
[11] K. Raghavachari, C. McMichael Rohlfing, J. S. Binkley, *J. Chem. Phys.* **1990**, *93*, 5862.
[12] G. E. Quelch, H. F. Schaefer III, C. Marsden, *J. Am. Chem. Soc.* **1990**, *112*, 8719.
[13] R. O. Jones, P. Ballone, *J. Chem. Phys.* **2003**, *118*, 9257.
[14] M. C. McCarthy, S. Thorwirth, C. A. Gottlieb, P. Thaddeus, *J. Chem. Phys.* **2004**, *121*, 632.
[15] M. H. Matus, D. A. Dixon, K. A. Peterson, J. A. W. Harkless, J. S. Francisco, *J. Chem. Phys.* **2007**, *127*, 174305.
[16] D. Coucouvanis, A. Hadjikyriacou, M. Draganjac, M. G. Kanatzidis, O. Ileperuma, *Polyhedron* **1986**, *5*, 349.
[17] R. Tegman, *Acta Crystallogr.* **1973**, *29*, 1463.
[18] M. W. Wong, Y. Steudel, R. Steudel, *Chem. Phys. Lett.* **2002**, *364*, 387.
[19] C. Mealli, A. Ienco, A. Poduska, R. Hoffmann, *Angew. Chem.* **2008**, *120*, 2906–2910; *Angew. Chem. Int. Ed.* **2008**, *47*, 2864.
[20] C. Mealli, A. Ienco, A. Messaoudi, A. Poduska, R. Hoffmann, *Inorg. Chim. Acta* **2008**, *361*, 3631–3637.
[21] J. T. York, E. C. Brown, W. B. Tolman, *Angew. Chem.* **2005**, *117*, 7923–7926; *Angew. Chem. Int. Ed.* **2005**, *44*, 7745–7748.
[22] Although a previous study[24] assigned a 1– charge to the S_4 ring, we will argue below that a better assignment is 2–. See also ref. [49]
[23] K. Isobe, Y. Ozawa, A. Vazquez de Miguel, T. W. Zhu, K. M. Zhao, T. Nishioka, T. Ogura, T. Kitagawa, *Angew. Chem.* **1994**, *106*, 1934; *Angew. Chem. Int. Ed. Engl.* **1994**, *33*, 1882.
[24] T. Nishioka, H. Kitayama, B. K. Breedlove, K. Shiomi, I. Kinoshita, K. Isobe, *Inorg. Chem.* **2004**, *43*, 5688.
[25] T. S. Lobana, K. Isobe, H. Kitayama, T. Nishioka, I. Kinoshita, *Angew. Chem.* **2004**, *116*, 215; *Angew. Chem. Int. Ed.* **2004**, *43*, 213.
[26] T. S. Lobana, K. Isobe, H. Kitayama, T. Nishioka, M. Doe, I. Kinoshita, *Organometallics* **2004**, *23*, 5347.
[27] T. Nishioka, S. Nakamura, Y. Kaneko, T. Suzuki, I. Kinoshita, S. Kiyooka, K. Isobe, *Chem. Lett.* **1996**, 911.
[28] C. Mealli, D. M. Proserpio, *J. Organomet. Chem.* **1990**, *386*, 203.
[29] R. D. Shannon, *Acta Crystallogr. A* **1976**, *32*, 751.
[30] S. Shaik, R. Hoffmann, *J. Am. Chem. Soc.* **1980**, *102*, 1194.
[31] S. Shaik, R. Hoffmann, C. R. Fisel, R. H. Summerville, *J. Am. Chem. Soc.* **1980**, *102*, 4555.
[32] C. Mealli, A. Orlandini, in *Metal Clusters in Chemistry*, *Vol. 1* (Eds.: P. Braunstein, L. A. Oro, P. R. Raithby), Wiley-VCH, New York, **1999**, p. 143.
[33] S. Alvarez, A. A. Palacios, G. Aullon, *Coord. Chem. Rev.* **1999**, *185–186*, 431.
[34] G. Aullon, M. Hamidi, A. Lledos, S. Alvarez, *Inorg. Chem.* **2004**, *43*, 3702.
[35] A. A. Palacios, G. Aullon, P. Alemany, S. Alvarez, *Inorg. Chem.* **2000**, *39*, 3166.
[36] J. Reinhold, O. Kluge, C. Mealli, *Inorg. Chem.* **2007**, *46*, 7142.
[37] Arising from the lowered symmetry in going from a square to a rectangle, we have mixing of the a_{2g} and b_{2g} orbitals to give two MO's that are either purely p_y or p_z.
[38] J. Martinez, H. Adams, N. A. Bailey, P. M. Maitlis, *J. Organomet. Chem.* **1991**, *405*, 393.
[39] *Gaussian 03*, M. J. Frisch, G. W. Trucks, H. B. Schlegel, G. E. Scuseria, M. A. Robb, J. R. Cheeseman, J. Montgomery, J. A. , T. Vreven, K. N. Kudin, J. C. Burant, J. M. Millam, S. S. Iyengar, J. Tomasi, V. Barone, B. Mennucci, M. Cossi, G. Scalmani, N. Rega, G. A. Petersson, H. Nakatsuji, M. Hada, M. Ehara, K. Toyota, R. Fukuda, J. Hasegawa, M. Ishida, T. Nakajima, Y. Honda, O. Kitao, H. Nakai, M. Klene, X. Li, J. E. Knox, H. P. Hratchian, J. B. Cross, V. Bakken, C. Adamo, J. Jaramillo, R. Gomperts, R. E. Stratmann, O. Yazyev, A. J. Austin, R. Cammi, C. Pomelli, J. W. Ochterski, P. Y. Ayala, K. Morokuma, G. A. Voth, P. Salvador, J. J. Dannenberg, V. G. Zakrzewski, S. Dapprich, A. D. Daniels, M. C. Strain, O. Farkas, D. K. Malick, A. D. Rabuck, K. Raghavachari, J. B. Foresman, J. V. Ortiz, Q. Cui, A. G. Baboul, S. Clifford, J. Cioslowski, B. B. Stefanov, G. Liu, A. Liashenko, P. Piskorz, I. Komaromi, R. L. Martin, D. J. Fox, T. Keith, M. A. Al-Laham, C. Y. Peng, A. Nanayakkara, M. Challacombe, P. M. W. Gill, B. Johnson, W. Chen, M. W. Wong, C. Gonzalez, J. A. Pople, Gaussian, Inc., Wallingford CT, **2004**.
[40] A. D. Becke, *J. Chem. Phys.* **1993**, *98*, 1372.
[41] C. Lee, W. Yang, R. G. Parr, *Phys. Rev. B* **1988**, *37*, 785.
[42] M. Dolg, H. Stoll, H. Preuss, R. Pitzer, *J. Phys. Chem.* **1993**, *97*, 5852.
[43] P. C. Hariharan, J. A. Pople, *Theo. Chim. Acta* **1973**, *28*, 213.
[44] C. Mealli, D. M. Proserpio, *J. Chem. Educ.* **1990**, *67*, 399.
[45] M. Doux, L. Ricard, P. Le Floch, Y. Jean, *Organometallics* **2006**, *25*, 1101.
[46] A. Ienco, M. J. Calhorda, J. Reinhold, F. Reineri, C. Bianchini, M. Peruzzini, F. Vizza, C. Mealli, *J. Am. Chem. Soc.* **2004**, *126*, 11954.
[47] A. L. Sargent, E. P. Titus, *Organometallics* **1998**, *17*, 65.
[48] G. Orlova, J. D. Goddard, *J. Phys. Chem. A* **1999**, *103*, 4078.
[49] Note added in proof: A recognized example of a S_4^{2-} bridging unit has recently appeared in the literature. S. Yao, C. Milsmann, E. Bill, K. Wieghardt, M. Driess, *J. Am. Chem. Soc.* **2008**, *130*, 13536.

Received: August 27, 2008
Published online: November 13, 2008

